THE JOURNAL OF PHYSICAL CHEMISTRY C

Article

pubs.acs.org/JPCC

Advancements in the Synthesis of Building Block Materials: Experimental Evidence and Modeled Interpretations of the Effect of Na and K on Imogolite Synthesis

Nicolás Arancibia-Miranda,[*,†,‡] Mauricio Escudey,[†,‡] Ricardo Ramírez,[§,‡] Rafael I. González,[∥,‡,⊥] Adri C. T. van Duin,[#] and Miguel Kiwi[∥,‡]

[†]Facultad de Química y Biología, Universidad de Santiago de Chile, Av. B. O'Higgins, 3363, Santiago, Chile

[‡]Center for the Development of Nanoscience and Nanotechnology (CEDENNA), 9170022 Santiago, Chile

[§]Facultad de Física, Universidad Católica de Chile, Casilla 306, Santiago, Chile 7820436

[∥]Departamento de Física, Facultad de Ciencias, Universidad de Chile, Casilla 653, Santiago, Chile 7800024

[⊥]Centro de Genómica y Bioinformática, Facultad de Ciencias, Universidad Mayor, Santiago, Chile

[#]Department of Mechanical and Nuclear Engineering, The Pennsylvania State University, University Park, Pennsylvania 16802, United States

Supporting Information

ABSTRACT: The effects of Na/K substitution during the synthesis of imogolite nanotubes (NTs) were studied using a combination of structural and surface analyses. These were complemented with molecular dynamics (MD) and DFT computational models. Our results provide strong experimental evidence, obtained by various characterization techniques (FT-IR, XRD, IEP, charge measurement, and HR-TEM), showing that K changes the imogolite dimensions. In fact, in the presence of K, the nanotubes become shorter and adopt a larger diameter. Moreover, the presence of the amorphous structures associated with allophane increases, even for low K concentrations. Our results underline the complexity of imogolite synthesis engineering, highlighting their high sensitivity to the chemicals that are used during synthesis.

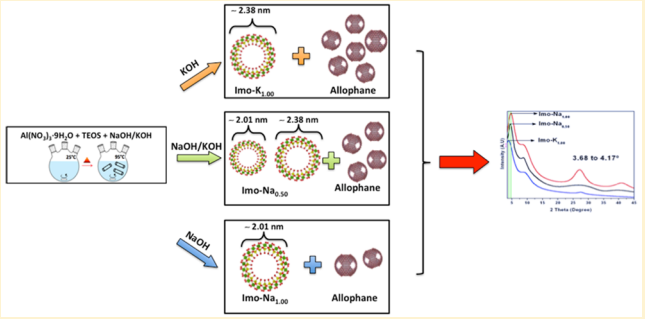

INTRODUCTION

The structure and dimension of engineered nanoparticles (ENP)[1−4] are critical factors because morphological modifications can substantially affect their physicochemical properties (electronic, optical, and mechanical properties), which reinforces the use of these types of materials.[2,5−7] The synthesis of different ENPs must consider the strict handling of a number of experimental factors (pH, temperature, chemical composition, initial reagent concentration, and others), which condition the morphology of the final product; consequently, insufficient control of the experimental factors can restrictively affect the potential technological applications of the products.[8,9]

The metal oxide nanotube family is a group that is considered to be essential for nanotechnology as building blocks. Imogolite, a nanotubular aluminosilicate (IMO), is a good example of a nanotube that can be studied from the perspective of nanoscopic or atomic engineering.[1,10,11] This paracrystalline aluminosilicate, in which the stoichiometry is $(OH)_3Al_2O_3SiOH$, was discovered in Japan in 1962 within soils of a volcanic origin, and it was first synthesized by Farmer et al. in 1977.[12,13] Imogolite is characterized by a hollow cylindrical structure with two clearly differentiated surfaces (Figure 1): an outer surface where aluminol (≡Al−OH and $\equiv Al_2-OH$) groups predominate and an inner surface mostly composed of silanol groups (≡Si−OH).[14−16]

These two nanosized structures have given rise to increasing scientific technological interest due to their easy production and high purity compared to other metal oxide nanotubes, considering that imogolite synthesis is usually carried out at temperatures no higher than 95 °C.[12,17−21] Their unique physicochemical properties, such as their well-defined wall structure, wide range of chemical compositions, porosity, tunable dimensions, and chemically modifiable inner and outer surfaces, allow us to utilize imogolite in multiple applications in the field of nanotechnology (e.g., catalysis, contaminant removal, sensor development, and molecular encapsulation).[5,22−24]

The chemical flexibility of imogolite becomes evident in the early stages of its synthesis. The replacement of −OH groups with gibbsite sheets by silicate (O_3SiOH), according to the

Received: December 2, 2016
Revised: May 28, 2017
Published: May 30, 2017

DOI: 10.1021/acs.jpcc.6b12155
J. Phys. Chem. C 2017, 121, 12658−12668

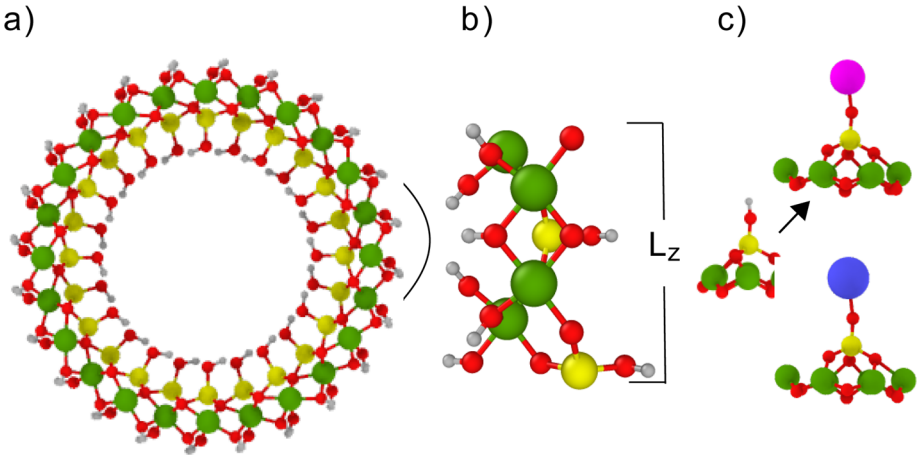

Figure 1. (a) Imogolite unit cell with $N = 12$ repetitions of the 28-atom circular sector, of angle $2\pi/N$, marked by the black continuous line. (b) Lateral view of the 28-atom structure angularly repeated to form imogolite. (c) DFT results for the structure illustrated on the left when H is replaced by Na (purple) and K (blue). Periodic repetitions of the unit cell are imposed in the axial direction. L_z is the axial length of the unit cell. H: light gray; O: red; Si: yellow; and Al: pink.

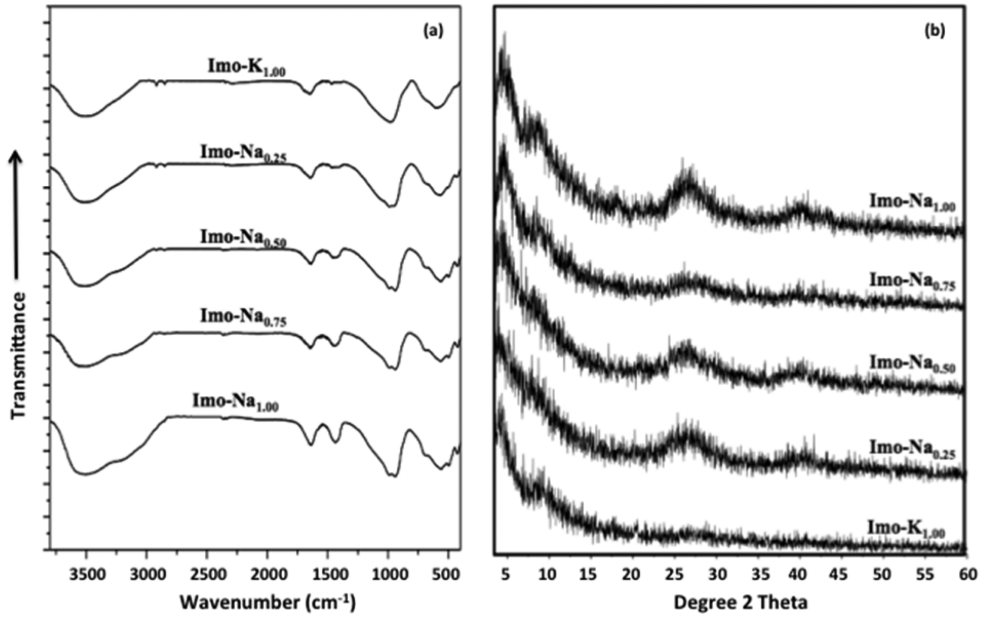

Figure 2. FTIR spectra (a) and experimental X-ray diffraction pattern of the synthetic imogolite synthesized in acidic solutions containing different amounts of NaOH and/or KOH (b).

model proposed by Cradwick et al. (1972),[25] causes a decrease in the bond length of the coordinating or bridge oxygen with this substituent, resulting in the curvature and superficial differentiation characteristics of these nanotubes.[26−28]

In spite of the advantages of imogolite, its formation, growth processes, and its dimensions are strongly influenced by factors such as temperature, pH, initial reagent concentration, and the presence of other ions.[20,29−31] The research of Abidin et al. suggests that the addition of NaCl or $CaCl_2$ during the synthesis of Na-imogolite partially inhibits its formation, suggesting that Ca^{2+} and an excess of Na^+ affect the dissociation of the Si−OH groups of orthosilicic acid.[32] Yucelen et al. made significant progress in nanoengineering aluminosilicates by showing that the presence of certain acids used (HCl, $HClO_4$, CH_3COOH) during the synthesis of imogolite enables the controlled modification of the outer diameter as a consequence of a specific relation between the precursors formed in the early stage of the synthesis and the final resultant structure.[33] Conversely, studies made on structures similar to imogolite, such as the aluminogermanates, have shown that it is possible to make controlled structural modifications from a physico-chemical standpoint, resulting in different kinds of nanotubes (single or double walled) by simply increasing the concentrations of the starting reagents.[3,29,33]

The synthesis of imogolite includes the hydrolysis of tetraethyl orthosilicate (TEOS) with NaOH, yielding a nanotube enriched product with exchangeable and structural Na. The presence of cations other than Na^+ with equivalent properties in the nanotubes can give rise to different applications; therefore, the main objective of this research was to evaluate the effect of substituting Na with K (NaOH by KOH) by the hydrolysis of TEOS during the synthesis of imogolite. We sought to produce nanotubes that are equivalent to those obtained in a Na medium but enriched with K. This is

DOI: 10.1021/acs.jpcc.6b12155
J. Phys. Chem. C 2017, 121, 12658−12668

the hydrolysis path responsible for the types of precursors that evolve into more complex structures during the aging process. An Na/(Na + K) ratio between 1 and 0 was evaluated in order to establish, at the molecular level, the roles of the monovalent cations in the formation of imogolite. The obtained materials were characterized in detail using multiple structural and superficial analysis techniques, in addition to computer models, which allow for an integrated interpretation of the results.

RESULTS AND DISCUSSION

Fourier transform infrared spectra of the aluminosilicates that were obtained from the different NaOH/KOH ratios were identified (Figure 2a). Differences in the spectra for the prepared products were observed in the imogolite peaks; KOH, in concentrations of $\sim 2.5 \times 10^{-4}$ mol L^{-1}, quenched the imogolite peaks, suggesting it conditioned the final products.[26,34] This behavior is similar to standard early synthesis stages already reported, where NP, amorphous structures, and proto-imogolite coexisted. Imogolite synthesized using NaOH as a hydrolysis agent (Imo-$Na_{1.00}$), displayed bands at 3300 and 3500 cm^{-1} that were associated with external ≡AlOH and ≡Al_2OH groups and stretching modes at 3615 cm^{-1} that corresponded to ≡Si−OH sites located in the inner surface of the imogolite (Figure 2a). For the aluminosilicate that was either partially or totally synthesized with KOH, bands of OH (3600 cm^{-1}), related to a globular structure that was most likely allophane, were observed.[15,25,35] The behavior observed in the −OH region has also been reported in other aluminosilicates, such as zeolites.[36]

When the imogolite synthesis is carried out using NaOH to provide the required alkaline conditions, a band at 1420 cm^{-1} associated with carbonate (CO_3^{2-}) is observed; that band is not observed when KOH (instead NaOH) is used. When NaOH chemical speciation is computational carried out, considering the regular dissolution of atmospheric CO_2, the formation of HCO_3^- and CO_3^{2-} may take place, at least from a thermodynamical point of view; this situation has been experimentally reported as NaOH carbonation.[37,38] The computational speciation of KOH in the same conditions does not report carbonate formation. This differentiated NaOH−KOH behavior may explain the presence (or absence) of the carbonate band observed for NaOH−imogolite in the IR spectra.

Another consequence of changing the cation, as observed in the IR spectra, was the progressive attenuation of the stretching Si−O vibration doublet at 990 and 939 cm^{-1}. This was a characteristic imogolite band that displayed its minimum intensity and was defined as Imo-$K_{1.00}$ for the 990, 939, 693, 570, 512, and 430 cm^{-1} bands.[15,25,35] Moreover, the 545, 388, and 372 cm^{-1} bands, related to variations of Al−OH, were affected.

X-ray diffraction was also implemented to evaluate the changes due to the different K and Na contents on the imogolite synthesis (Figure 2b). Four Imo-$Na_{1.00}$ diffuse peaks were observed at 21.0, 12.0, 3.4, and 2.2 Å, with the (*hkl*) planes corresponding to (100), (110), (001), and (211), respectively, that were characteristic of this aluminosilicate, suggesting that they were ordered in either monoclinic or hexagonal arrangements.[14,33,39,40]

The signal intensity and the low-angle peak positions changed in the samples synthesized, partially or totally, with KOH. This indicated that K modified two imogolite characteristics: first, the internal diameter and the number of byproducts and, second, the signal intensity becomes more noticeable as the K content increases, reaching a maximum for Imo-$K_{1.00}$, as illustrated in Figure 1b. The increasing K content in the sample resulted in peak displacement, which correlated to the external diameter of the imogolite (3.68° to 4.17° for the (*hkl*) reflection (100)).[40] While for the sample synthesized using equimolar concentrations of NaOH and KOH (Imo-Na0.50), the observed peak displacement (100) was the result of the contributions of the imogolite nanotubes formed from each base used (see Figure 1S). These results were not conclusive for the NTs that displayed different diameters, which were identified as several NTs fastened together. However, taken globally, the evidence was quite compelling.

Figure 3 shows that imogolite synthesized with different NaOH/KOH ratios had slightly larger diameters and lengths when compared with those obtained using only NaOH. Moreover, the presence of spherical morphology byproducts (allophane) determined the type and structure of the early aging stages.[14] For the different products, the particle diameter was estimated from an average of >100 ($p < 0.05$, *t* test, sample size >100 nanoparticles) measurements at different scales and defined by a super-resolution analysis of the images. The diameter trend follows the sequence $2.01 \leq 2.05 < 2.20 < 2.28 < 2.38$ nm for Imo-$Na_{1.00}$, Imo-$Na_{0.75}$, Imo-$Na_{0.50}$, Imo-$Na_{0.25}$, and Imo-$K_{1.00}$. Two NT families of different diameters and lengths were observed in the samples synthesized with a NaOH-KOH mixture, suggesting that the dimensions and structural growth of the imogolite base structures were conditioned by the presence or absence of Na and/or K. NTs with variable diameters of the Imo-Na_xK_{1-x} type were not obtained, which suggested that slight precursor structural differences required larger energies to create these mixed NTs. Moreover, these results, along with the XRD results, confirmed that K did modify the Imo-$K_{1.00}$ diameter, which increased by ~20% compared to Imo-$Na_{1.00}$.

The NT length diminished as the K concentration increased, reaching approximately 70 nm for Imo-$K_{1.00}$, confirming that K inhibited the NT growth along the tube axis.

A liquid-phase spectroscopic analysis (UV−vis) was performed on all the differently aged samples. In parallel, the initial reactive chemicals and the final solutions were evaluated as well as a synthetic allophane solution with an Al/Si ratio similar to that of the imogolite (Figure 4).

The spectra evidence the time evolution and changes in the peak definition as a function of time. In Figure 4, the maximal dispersion of the 262 and 304 nm peaks is observed; they are related to the globular and cylindrical aluminosilicate structures such as allophane and imogolite, respectively.[1,10,41] During the initial stages of the synthesis process an enhanced amount of K was present in the solution. The allophane content increased, and consequently, the allophane signal (at 262 nm) also increased significantly. Simultaneously, the 304 nm peak only slightly changed. This behavior is consistent with previous research because imogolite formation only occurs during the later synthesis stages (after more than 24 h).

After the aging time (120 h), and on the basis of the data obtained from the UV−vis spectra, at a concentration of KOH of $\sim 1.0 \times 10^{-3}$ M (Imo-$K_{1.00}$), the formation of two products was favored: allophane and imogolite in practically equivalent amounts. Instead, Imo-$Na_{1.00}$ allophane only formed in marginal amounts. This data is consistent with the TEM observations (Figure 3). A different behavior was observed when the maximal dispersion 304 nm signal, associated with the

DOI: 10.1021/acs.jpcc.6b12155
J. Phys. Chem. C 2017, 121, 12658−12668

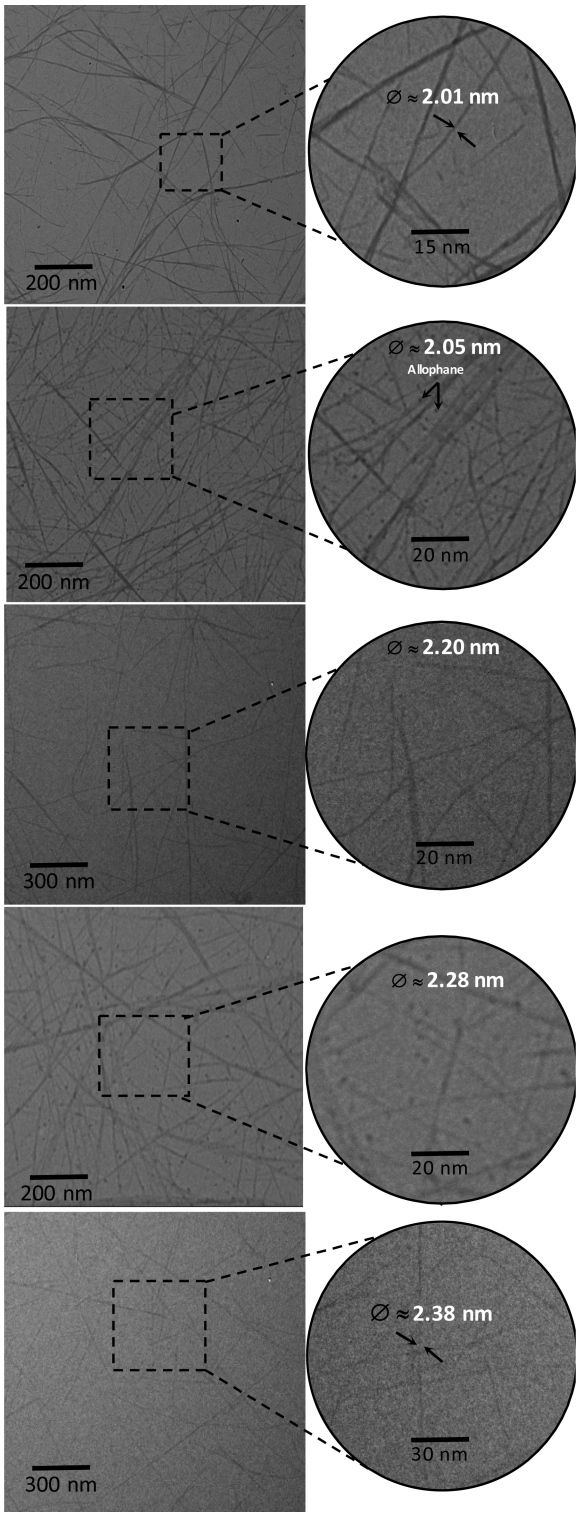

Figure 3. Representative low- and high-magnification HR-TEM images of imogolite: (a, b) Imo-$Na_{1.00}$; (c, d) Imo-$Na_{0.75}$; (e, f) Imo-$Na_{0.50}$; (g, h) Imo-$Na_{0.25}$; and (i, j) Imo-$K_{1.00}$.

imogolite concentration as a function of aging over time, was monitored. The latter suggests the existence of multiple dynamic optical phenomena that occurred as a function of time, similar to what Mukherjee et al. reported for alumino-germanate NTs.[1] In general, the content of K generated a larger number of amorphous NPs, which mainly led to allophane. This aluminosilicate formed immediately after the initial mixing process but did not produce imogolite, since the latter required a highly complex restructuring process that was strongly conditioned by aging time and temperature.[11,42,43]

Imogolite NT Surface Changes Related to the NaOH/KOH Ratio. The isoelectric point (IEP) is a parameter that is highly sensitive to the surface changes that occur in these materials.[14,16] The IEP was obtained using electrophoretic mobility techniques (Figure 5). Recently, Arancibia-Miranda et al. determined variations in the imogolite IEP values for various synthesis routes that were related to a single step in the process, namely, the partial acidification of the precursors.[14] IEP values between 9.2 and 10.5 were obtained, which, due to the lack of acidification of the precursors, were attributed to the increased allophane content.[3,15]

To shed light on how Na and K impacted the surface charge and composition of the different imogolite synthesis products, several additional IEP measurements were performed. The IEP at the end of the synthesis, after 120 h, is shown in Figure 5a. It was observed that the IEP decreased as the K content increased, reaching 8.60 ± 0.02 for Imo-$K_{1.00}$, which was almost 2.5 pH units lower than the 11.05 ± 0.02 determined for Imo-$Na_{1.00}$.

Figure 5b shows the pH variation as a function of time and the Na and K content. At the end of the initial reactive mixing process, the pH values for Imo-$Na_{1.00}$ and Imo-$K_{1.00}$ were 3.85 and 4.60, respectively, which evidenced the different chemical precursor environments. These differences were related to the allophane presence during the synthesis with NaOH/KOH, as described in the literature.[14,15] These surface and structural changes, associated with pH variations, were due to the various oxolation processes reported during the evolution and formation of the imogolite.[11,15,44] Each stage of the imogolite synthesis process releases protons.[15] Thus, the more the synthesis progresses, the more protons are released with the consequent drop in pH.[14,15] The synthesis of imogolite made in NaOH medium is completed to a much greater degree than the synthesis made in KOH medium; consequently, the final pH of the suspension will be more acidic when done in sodium medium than when done in potassium medium. This indicated that the precursor formation and subsequent assemblies of more complex structures required the liberation of H^+. This was not the case for Imo-$Na_{0.25}$ and Imo-$K_{1.00}$. A more significant way of observing the effect of the structural changes on the pH was to represent the variation of this parameter as a function of aging over time (Figure 5b, inset).

Recently Levard et al. studied the effect of different hydrolysis ratios (from n_{OH}/n_{Al} = 0.5 to 3) on the synthesis of Ge-imogolite, finding that this parameter is conditional to the type of structure precursor to the formation of this nanotube, where n_{OH}/n_{Al} > 2.0 generated structural defects or inhibition of Ge-imogolite. Taking into account that result, it is possible to assume that the same n_{OH}/n_{Al} ratio may have a different effect on imogolite synthesis when done in Na or K medium.[19,45]

This behavior suggested that the presence of KOH caused the Al intermediates to form more thermodynamically stable polymers that are not optimal for the formation of imogolite, such as $Al_{13}O_4(OH)_{24}(H_2O)_8^{4+}$, as previously proposed by Wilson et al. In addition, KOH affected the SiO_4^{4-} formation because the base might have been involved in the TEOS hydrolysis.[27]

The surface charge studies shed light, at a macroscopic level, on the synthesis differences between the Na and K processes,

DOI: 10.1021/acs.jpcc.6b12155
J. Phys. Chem. C 2017, 121, 12658−12668

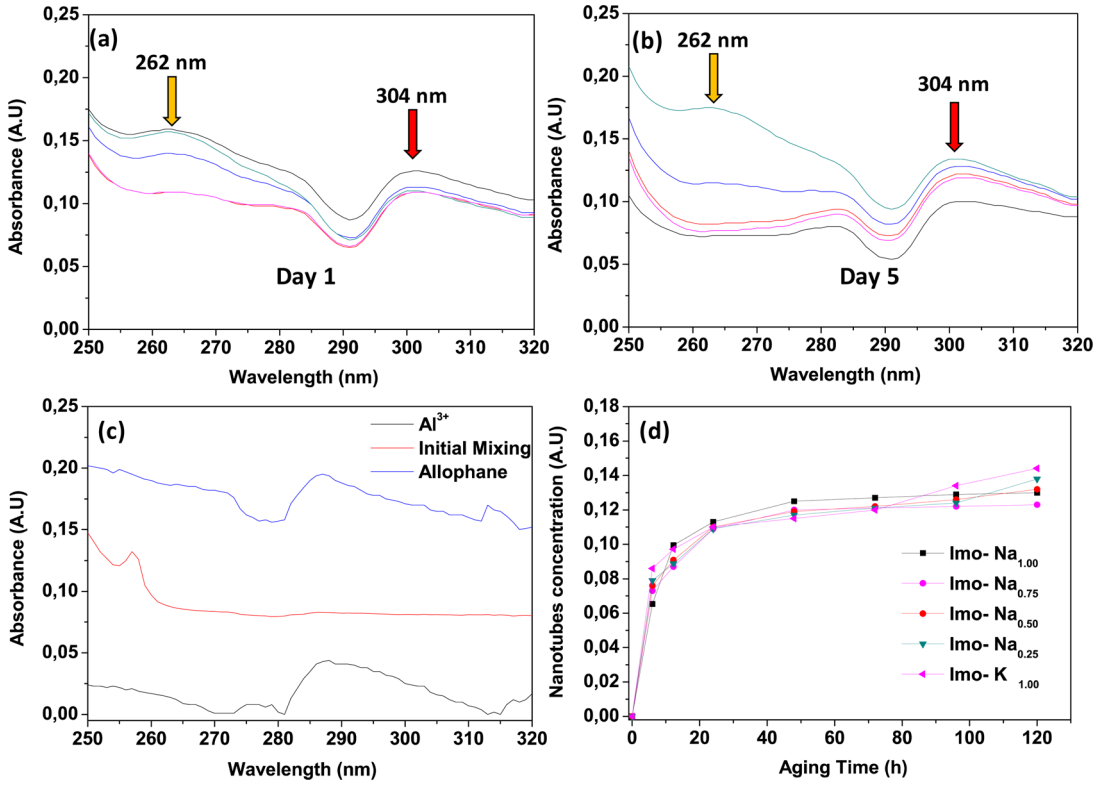

Figure 4. UV−vis spectra of the solutions at various times during the reaction at 95 °C. (a) One-day aging. (b) Five-day aging. (c) Allophane and reactants. (d) Concentration of the nanotubes, obtained from 304 nm excitation as a function of the growth time.

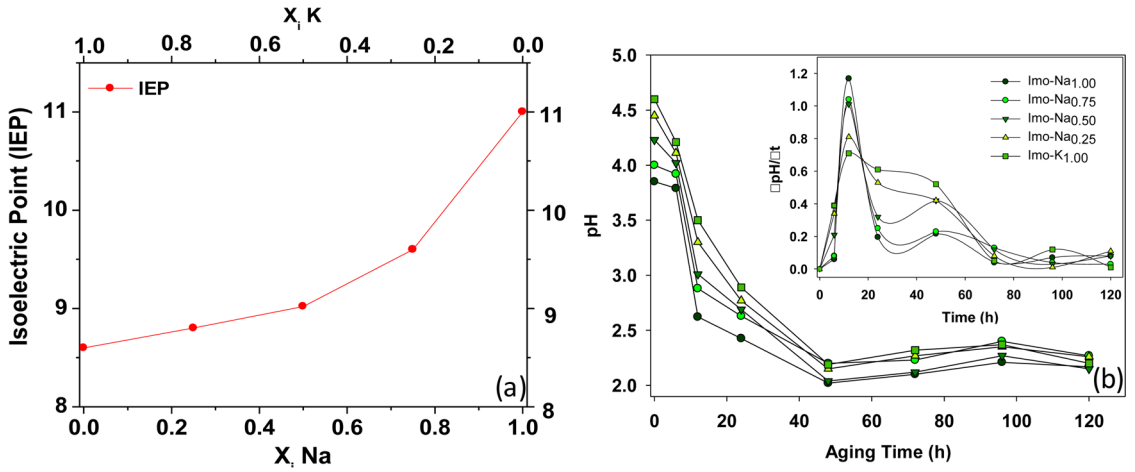

Figure 5. (a) Isoelectric point vs NaOH/KOH ratio for the different final products obtained after 120 h and (b) pH change of the nanotube synthesis solution as a function of the reaction time and Na and K content. The inset illustrates the differential pH as a function of aging with time ($\Delta pH_a/\Delta t$ vs aging time).

on the basis of the internal and external surface compositions. In fact, the behavior of silica, which was representative of the inner active sites (≡Si−OH), and of alumina, which was representative of the external sites (≡Al−OH and ≡Al_2−OH), contributed to our understanding of the differences. The surface dissociation constants and surface complexation constants were determined from potentiometric titration data by applying the triple-layer model (TLM), developed by Davis and co-workers.[46−49] The surface charge dissociation constants (K_{a1} and K_{a2}) and the cationic and anionic complexation constants ($^*K_{a1}$ and $^*K_{a2}$) are described by eqs 1−4.

$$SOH_2^+ \leftrightarrow SOH + H^+ \quad Ka_1 = \frac{(SOH)(H^+)}{(SOH_2^+)} \exp(-e\Psi_o/kT) \tag{1}$$

$$SOH \leftrightarrow SO^- + H^+ \quad Ka_2 = \frac{(SO^-)(H^+)}{(SOH)} \exp(-e\Psi_o/kT) \tag{2}$$

$$SOH + H^+ + Cl^- \leftrightarrow SOH_2^+{-}Cl^-{*}$$
$$Ka_1 = \frac{(SOH)(Cl^-)(H^+)}{(SOH_2^+{-}Cl)} \exp(-e(\Psi_o - \Psi_\beta)/kT) \tag{3}$$

DOI: 10.1021/acs.jpcc.6b12155
J. Phys. Chem. C 2017, 121, 12658−12668

$$SOH + M^+ \leftrightarrow SOH^- - M^+ + H^{+*}$$

$$Ka_2 = \frac{(SOH^- - M^+)(H^+)}{(SOH)(M^+)} \exp(-e(\Psi_o - \Psi_\beta)/kT) \quad (4)$$

where M^+ corresponds to Na^+ or K^+, represented by the "o" symbols on the left side, and β represents the plane of the outer-sphere complexes. The activity of the protons located in the superficial plane (H^+_o) is related to the activity of the protons in the solution through the Boltzmann equation (eq 5).

$$(H^+_o) = (H^+) \exp(-e\Psi_o/kT) \quad (5)$$

In a similar way, the activity of the cations and anions forming the outer-sphere complexes is also related to the activity in the solution phase by eqs 6 and 7:

$$(M^+_\beta) = (M^+) \exp(-e\Psi_\beta/kT) \quad (6)$$

$$(Cl^-_\beta) = (Cl^-) \exp(-e\Psi_\beta/kT) \quad (7)$$

The dissociation constants (K_{a1} and K_{a2}) provide information on the distribution of the positive, neutral, and negatively ionized sites as a function of pH. The complexation constants ($^*K_{a1}$ and $^*K_{a2}$) provide information on the anion (Cl^-) and cation (Na^+ or K^+) interactions with the surface.

In Figure 6, as an example, the potentiometric titration curves carried out at I = 0.1 M KCl are shown. From these curves, the PZNPC and, by applying the TLM, the surface dissociation and complexation constants were determined (Table 1).

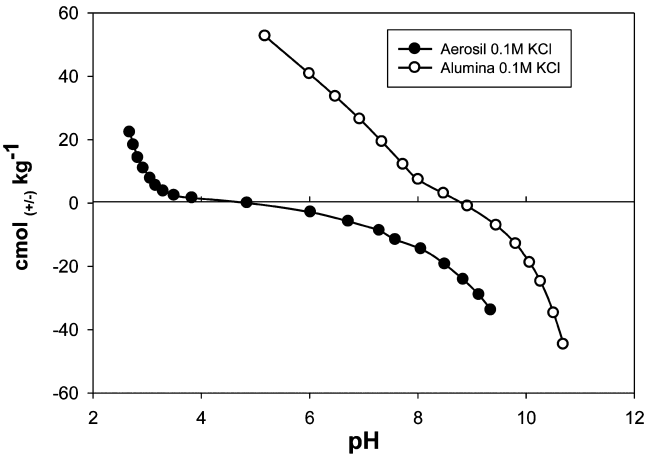

Figure 6. Potentiometric titration curves carried out at I = 0.1 M KCl and 25 °C for alumina (Al_2O_3) and aerosil (SiO_2).

The PZNPC values for silica (aerosil) and alumina were within the values reported for similar materials when the point of zero charge was determined through pH measurements.[50] Only slight differences between NaCl and KCl were observed (0.2−0.3 pH units), confirming the characteristics of the outer-sphere complexes formed by both electrolytes.

The intrinsic dissociation constants were related to the deprotonation from SOH_2^+ to SOH (K_{a1}) and SOH to SO^- (K_{a2}) and clearly accounted for the more acidic surface active sites of silica and the more alkaline surface active sites of alumina. The data agree with the expected relationship of PZNPC = 0.5(pK_{a1} + pK_{a2}). From the intrinsic complexation constants ($^*K_{a1}^{int}$, $^*K_{a2}^{int}$), it was possible to estimate the interactions of Na^+ and K^+ with the surface by quantifying the free energy involved in the process, as shown in Table 1. When the electrolyte changed from Na^+ to K^+, 7.7% less energy was required to approach the surface of the Si−OH groups, but 23.3% more energy was required for K^+ to approach the surface of Al−OH. Thus, from a macroscopic point of view, the difference in the free energy when NaCl changed to KCl as the electrolyte during the procedure to synthesize imogolite may explain the differences observed. Thus, in NaCl, mostly imogolite was obtained; in KCl, allophane and gibbsite were the most important products of the same procedure.

Modeling the Effect of the NaOH/KOH Ratio on the Imogolite Formation. The analysis of our results shows that K generated several effects on the imogolite formation since the byproduct (allophane) quantity and the NT length were influenced by it. The presence of K accelerated the allophane kinetics since it formed as soon as the reactants were mixed, favoring the formation of allophane over imogolite. This could be due to the different TEOS hydrolysis speeds for different NaOH/KOH ratios, which generated a differential between Al and Si that resulted in precursors (proto-imogolites) that were not prone to properly reorder as imogolite. Since the reordering process during aging was endothermic, this suggested that K tended to quench the system, favoring allophane, a product with less energy demand than imogolite.[14,39,45] This would explain the loss in crystallinity of the XRD spectra and the IEP and pH changes.

In this way, the morphological differences between Imo-$Na_{1.00}$ and Imo-$K_{1.00}$ originated during the formation of the early precursors that led to the final imogolite raft structure. K slightly changed the angles of these structures as a consequence of their smaller sized hydrated radius (232 pm) compared to that of Na (276 pm). The K surface group energy differences, mainly due to ≡Si−OH (Table 1), also contributed (Figure 7). These characteristics led to different curvatures of the proto-imogolite clusters, a similar behavior has been reported in the literature.[3,33]

Classical Molecular Dynamics Results. A synthetic procedure for the preparation of monodisperse imogolite remains elusive. From the point of view of the computational models, a minimum of the strain energy has been reported as a

Table 1. Point of Zero Net Proton Charge (PZNPC), Surface Charge Dissociation (pK_{a1}^{int}, pK_{a2}^{int}) and Complexation Constants ($p^*K_{a1}^{int}$, $p^*K_{a2}^{int}$), and Free Energy ($\Delta G°$) Involved for Aerosil and Alumina in KCl and NaCl

electrolyte	PZNPC	pK_{a1}^{int}	pK_{a2}^{int}	$p^*K_{a1}^{int}$	$p^*K_{a2}^{int}$	$\Delta G°$ (kcal mol^{-1}) Cl^-	$\Delta G°$ (kcal mol^{-1}) M^+
				aerosil 200 (SiO_2)			
KCl	4.9	2.6	7.3	2.8	7.0	3.8	9.5
NaCl	4.7	1.8	7.7	1.8	7.6	2.5	10.3
				alumina girdler (Al_2O_3)			
KCl	8.7	7.2	10.4	7.1	10.5	9.6	14.3
NaCl	8.4	6.5	10.0	7.8	8.5	10.6	11.6

DOI: 10.1021/acs.jpcc.6b12155
J. Phys. Chem. C 2017, 121, 12658−12668

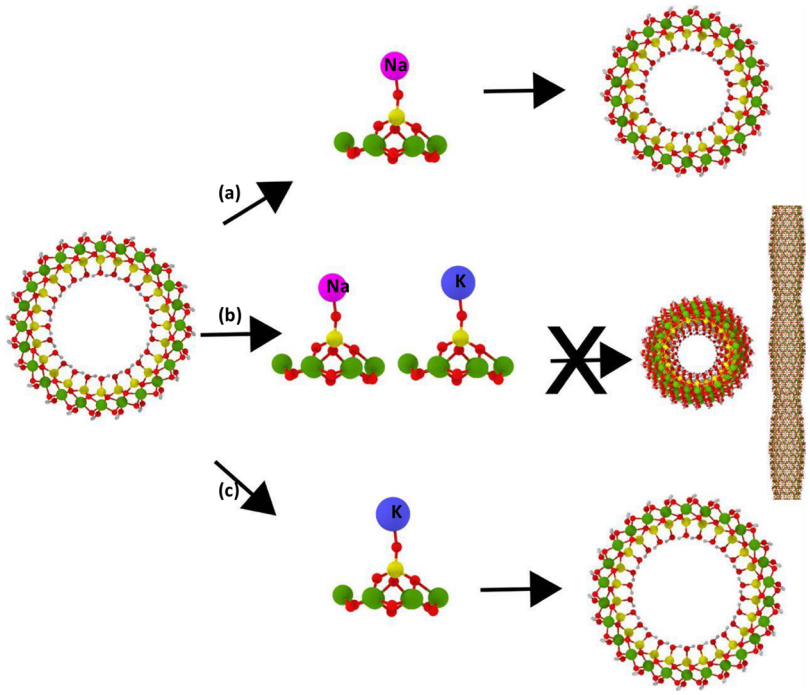

Figure 7. Shape of the metal oxide nanotubes. Cation effect: (a) 100% Na, (b) Na + K mixture, and (c) 100% K.

function of the diameter of the nanotube as the main key factor for obtaining monodispersity.[51−53] However, Yucelen et al. showed that modification in the synthetic procedure leads to N = 11−15, which results in values that are much higher than those predicted.[42,56] Finally, Lourenco et al. showed that the energy minimum for Ge-Imogolite (total replacement of Si by Ge) was much larger than that of pure imogolite.[56] This aligned well with experimental data for the Ge-imogolite nanotubes of ≈1 nm.[10,25] Thus, it can be interpreted that the diameter of the minimum energy found in the theoretical models is lower than the diameter that can be obtained from bench work. In this work, we replaced the H atoms of the inner wall of the nanotube for K or Na atoms and calculated the power of the nanotube as a function of energy. This was a simplified model to understand, by means of computational modeling, the effect of the use of NaOH or KOH during the synthesis process.

The results of our simulations are shown in Figure 8. H-Imo, Na-Imo, and K-Imo correspond to the classical Na- and K-replaced imogolite structures, respectively. For H-Imo, an energy minimum of N = 8 was obtained, which was very close to the N = 9 value. The diameter decreased within the range N = 8−12, similar to values previously reported.[51−53] We also adjusted the size of the box along the imogolite axis and obtained, for the length of the unit cell, 8.55 Å for N = 7 and 8.8 Å for N = 10, which were also quite close to other theoretical results in the literature that were between 8.40−8.84 Å and the experimental results of 8.4−8.5 Å.[10,52,55,57,58]

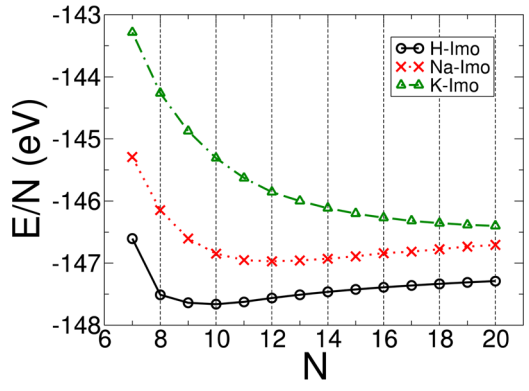

Figure 8. Thermodynamic average of E/N vs the number of repetitions of the angular sector (Figure 1). The values were obtained using the ReaxFF.

When replacing the H atoms in the inner wall of the NT by Na or K, the total energy increased, and the energy minimum was shifted to N = 11 and N = 18, respectively. Which meant that, first, the results were energetically more favorable for NTs with H than with Na or K as a final product of the synthesis, and second, we expected it to be less probable to obtain imogolite NTs using K than Na. Finally, making a connection between the present results and the work by Yucelen et al., it appeared to be possible to tune the NT diameter by means of the precursors.[33]

Quantum Treatment Results. The curling of gibbsite, leading to the formation of imogolite, occurs when a SiOH group located in a vacant octahedral gibbsite site forms SiO_4 tetrahedrons. This process requires a shortening of the O−O bonds around the vacant site, which in turn causes the gibbsite sheet to curl.[25,34,59]

The SiO bond pointing out of the sheet is neutralized by the proton. In practice, synthesis of imogolite is controlled by the addition of small amounts of alkali and alkaline-earth metal ions, which replace the protons and play the same role. However, as discussed above, Na and K have different effects on the formation of an imogolite tube. One can conjecture that these alkali metals differently affect the curling process in such a way that the use of K makes imogolite formation less probable. To test this hypothesis, a simple model was used which consisted of a small section of the proto-imogolite, as shown in Figure 1c. The geometrical optimization of this structure was performed in the case of Na and in the case of K. The sole

DOI: 10.1021/acs.jpcc.6b12155
J. Phys. Chem. C 2017, 121, 12658−12668

purpose of this calculation was to determine whether Na and K differently affected the formation of the orthosilicate structure. To prevent a disarray of the original geometry and to keep its general shape, the optimization was done in two steps. First, *z*-coordinates were kept fixed while the other two were free to move, and second, the optimization was done in the opposite order.

The results of these simulations are shown in Table 2, which shows that both tetrahedra were very similar. The same results are illustrated in Figure 1c, where the green circles represent aluminum atoms and A (yellow) represents a Si atom. The labels B, C, D, and E are the neighboring oxygen atoms. These results show that both Na and K had the same effect on the formation of the orthosilicate. One can conclude that these metals played a different role in the kinetics of the process and not in the curling process of the proto-imogolite.

Table 2. Bond Lengths (in Å) and O−Si−O Angles (in deg) for Imo-$Na_{1.00}$ and Imo-$K_{1.00}$[a]

bond	Na	K
AB	1.6265	1.6263
AC	1.7190	1.7196
AD	1.7335	1.7382
AE	1.5650	1.5662
angle	Na	K
BAC	102.93	102.45
CAD	102.01	102.81
DAB	104.21	104.33
BAE	114.80	115.02
CAE	114.23	114.65
DAE	116.87	114.65

[a]A labels a Si atom, and B, C, D, and E are the nearest-neighbor O atoms.

CONCLUSIONS

The effect of K^+ and Na^+ (KOH and NaOH) during the synthesis of imogolite was investigated experimentally from a structural and superficial point of view. The results were validated by macroscopic modeling and computational techniques (molecular dynamics and DFT). The experimental results revealed a reduction in the crystallinity, changes in the IR bands, and a displacement of the IEP toward more acid pH values when the synthesis procedure moved from 100% NaOH to 100% KOH. These facts were associated with the increasing allophane-type amorphous structures that were produced as a byproduct during the imogolite synthesis.

The dimensions of the nanotubes, estimated on the basis of an HR-TEM analysis, showed a slight diameter increase, but a significant reduction in the length of the imogolite synthesized in the presence of KOH was observed, compared to the imogolite obtained with 100% NaOH. No synthesis conditions could be found for the formation of nanotubes with a nonconstant diameter, an indication that their formation was energetically unfavorable. The TLM method allowed a macroscopic approach to the various systems that were studied, thus providing a mechanistic and experimental support for the different interactions among the active sites involved in the synthesis of imogolite with both cations (Na^+ and K^+).

The numerical calculations confirmed that the synthesis of imogolite using KOH was not energetically favored and that K^+ did slightly modify the bond lengths and angles of the imogolite precursors when compared to the NaOH synthesis; this energy barrier and the geometry changes were the main causes of the byproducts, such as allophane (which required less formation energy), and of the diameter changes of the KOH prepared imogolite.

This study proved that the synthesis of engineered imogolites is a complex matter. Moreover, it depends critically on the chemicals considered during the synthesis procedure and their relevance for potentially modifying the imogolite at a molecular scale.

MATERIALS AND METHODS

Synthesis of Imogolite. Imogolite was synthesized using the procedure described by different authors.[12,19] Briefly, tetraethyl orthosilicate (TEOS) was added to an aqueous solution containing 5 mM $AlCl_3$ until an Al/Si ratio of 2:1 was achieved. The TEOS hydrolysis was performed slowly by adding a 0.01 mol L^{-1} solution of NaOH:KOH in the following proportions: 1:0, 3:1, 1:1, 1:3, and 0:1, until an ^-OH/Al ratio close to 2 was obtained. The mixture was stirred overnight and heated at 95 °C in an oven for 5 days. Then, the maximum yield of imogolite was reached for the regular procedure.

Characterization Methods. The imogolite samples were characterized using Fourier transform infrared spectroscopy (FT-IR; Tensor 27 Bruker spectrometer). Dry samples (3.0 mg) were pressed into a spectral-grade KBr matrix for the measurements. Each spectrum was obtained by scanning the sample 32 times, with a spectral resolution of 2 cm^{-1}.

X-ray diffraction data were collected on a Philips X'Pert diffractometer with graphite-monochromated Cu Kα radiation, using oriented aggregates, which were prepared by drying water suspensions of the samples on glass slides.

For UV−vis analyses, 5 mL samples were withdrawn from the reactor and filtered through a 0.2 mm pore size syringe filter to produce a dust-free sample containing only nanoparticles (NPs). The UV−vis data were obtained on a Thermo Helios α UV−vis spectrometer. A quartz cuvette was used as a sample holder because it was optically transparent to UV radiation. The sample morphologies were observed with a Zeiss EM-910 transmission electron microscope (HR-TEM) at an acceleration potential of 80 kV, equipped with an Olympus Megaview digital camera (Olympus, Ontario, Canada). Data analysis was performed on 1376 × 1096 pixels images. Size/pixel resolution was calculated as ∼0.72 nm/pixel in ImageJ software. A thin layer of carbon was deposited on the surface by vacuum evaporation, and the carbon/product film was separated from the mica sheet by floating on distilled water. The separated film was subsequently transferred to a perforated Cu support grid for TEM measurements. The samples were acidified (0.01 mol L^{-1} HCl) to improve the imogolite dispersion and to minimize the presence of allophane.

The isoelectric point (IEP) was determined using electrophoretic mobility (EM) data, which were acquired using a Zetameter System 4.0. The imogolite samples (∼100 mg) were suspended in 200 mL of aqueous solution with an ionic strength of 5.0 mmol L^{-1}, and the EM was determined as a function of pH. From the plot of EM versus pH, the value of IEP was obtained by determining the pH value at which EM = 0. The pH of each suspension was adjusted by adding 0.01 mol L^{-1} of HCl or XOH (where X = Na^+ or K^+).

The potentiometric titration was carried out with a suspension of 300−400 mg of solids in 100 mL of 10^{-1} mol L^{-1} KCl or NaCl equilibrated for 1 h and then titrated with

DOI: 10.1021/acs.jpcc.6b12155
J. Phys. Chem. C 2017, 121, 12658−12668

aliquots of 0.1 M XOH (where X = Na^+ or K^+) or HCl every 10 min while recording the pH changes. The titration blanks were similarly obtained using 100 mL of KCl or an NaCl solution of an appropriate concentration. Titrations were carried out at 25.00 ± 0.01 °C, and the pH responses of the electrode were calibrated with buffer solutions of pH 4.0, 7.0, and 10.0. For each pH, the net charge density was calculated by the following expression:

$$\sigma = (\Gamma_{H+} - \Gamma_{OH-}) \quad (8)$$

where $\Gamma_{H+} - \Gamma_{OH-}$ represent the concentrations (cmol kg^{-1}) of H^+ and OH^- interacting with the sample surface.

Quantum Molecular Dynamics. The geometry optimization of the structures was performed using a DFT formalism, as implemented in the VASP code,[60,61] with pseudopotentials of the projected augmented wave (PAW) and the exchange-correlation parametrization given by Perdew et al..[62] For the dynamics, the plane wave cutoff was set to 150 eV. To avoid self-interactions, a rectangular cell with sides of 15 × 15 × 25 Å was used, with the longest side along the *z*-axis. The energy cutoff was set at 150 eV.

Classical Molecular Dynamics: Simulation Details. Classical Molecular Dynamics (MD) simulations with the Large-scale Atomic/Molecular Massively Parallel Simulator (LAMPS) code were used.[63] The atomic interactions were modeled with the ReaxFF potential,[64] parametrized against the interaction of the solute with organic molecules and tested.[65−68] We chose to use the Fast Inertial Relaxation Engine (FIRE) in combination with conjugate gradient minimizations to optimize the nanotube (NT) conformation and the length of the simulation cell, with encouraging results.[55] The LAMMPS implementation of FIRE does not allow you to vary the length of the simulation box; however, it does implement conjugate gradients. On the other hand, FIRE yields lower energy structures. Because of these reasons, both methods combined the cell length and structural optimization successively and repeatedly to achieve both better conformations and cell lengths. For the imogolite structure, a model proposed by Cradwick et al. with $7 \leq N \leq 20$ values was adopted.[25,64] Periodic boundary conditions along the tube axis and free boundaries along the other two dimensions were used. Because ReaxFF has a cutoff radius of 10 Å, we used three repetitions of the imogolite unit cell to ensure that we had a box longer than 20 Å along the periodic axis. We repeated the same procedure but replaced the inner H with Na and K. The charge equilibrium was checked at every geometrical optimization step.

■ ASSOCIATED CONTENT

Supporting Information

The Supporting Information is available free of charge on the ACS Publications website at DOI: 10.1021/acs.jpcc.6b12155.

Detailed XRD and ReaxFF parameters (PDF)

■ AUTHOR INFORMATION

Corresponding Author

*(N.A.-M.) E-mail: nicolas.arancibia@usach.cl.

ORCID

Nicolás Arancibia-Miranda: 0000-0002-0142-6922

Notes

The authors declare no competing financial interest.

■ ACKNOWLEDGMENTS

This work was supported by Fondo Nacional de Investigaciones Científicas y Tecnológicas (FONDECYT, Chile) under grants 11130157, 1160639, 1130272, and 3140526 and CEDENNA through Financiamiento Basal para Centros Científicos y Tecnológicos de Excelencia-FB0807. A.C.T.v.D. acknowledges funding from NSF DMR grant 1609107. This work was partially supported by the Laboratory Directed Research and Development (LDRD) program of Sandia National Laboratories. Sandia National Laboratories is a multimission laboratory managed and operated by Sandia Corporation, a wholly owned subsidiary of Lockheed Martin Corporation, for the U.S. Department of Energy's National Nuclear Security Administration under contract DE-AC04-94AL85000. We are especially grateful to Drs. Mi Umius and Martin Treps for their technical assistance.

■ REFERENCES

(1) Mukherjee, S.; Kim, K.; Nair, S. Short, Highly Ordered, Single-Walled Mixed-Oxide Nanotubes Assemble from Amorphous Nanoparticles. *J. Am. Chem. Soc.* **2007**, *129*, 6820−6826.

(2) Zang, J.; Konduri, S.; Nair, S.; Sholl, D. S. Self-Diffusion of Water and Simple Alcohols in Single-Walled Aluminosilicate Nanotubes. *ACS Nano* **2009**, *3*, 1548−1556.

(3) Thill, A.; Maillet, P.; Guiose, B.; Spalla, O.; Belloni, L.; Chaurand, P.; Auffan, M.; Olivi, L.; Rose, J. Physico-Chemical Control over the Single- or Double-Wall Structure of Aluminogermanate Imogolite-like Nanotubes. *J. Am. Chem. Soc.* **2012**, *134*, 3780−3786.

(4) Arancibia-Miranda, N.; Escudey, M. *Nanosized Tubular Clay Minerals*; Yuan, P., Thill, A., Begaya, F., Eds.; Elsevier: Amsterdam, 2016; Vol. 7, pp 458−465.

(5) Kang, D.-Y.; Brunelli, N. A.; Yucelen, G. I.; Venkatasubramanian, A.; Zang, J.; Leisen, J.; Hesketh, P. J.; Jones, C. W.; Nair, S. Direct Synthesis of Single-Walled Aminoaluminosilicate Nanotubes with Enhanced Molecular Adsorption Selectivity. *Nat. Commun.* **2014**, *5*, 3342.

(6) Konduri, S.; Mukherjee, S.; Nair, S. Controlling Nanotube Dimensions: Correlation between Composition, Diameter, and Internal Energy of Single-Walled Mixed Oxide Nanotubes. *ACS Nano* **2007**, *1*, 393−402.

(7) Levard, C.; Masion, A.; Rose, J.; Doelsch, E.; Borschneck, D.; Olivi, L.; Chaurand, P.; Dominici, C.; Ziarelli, F.; Thill, A.; et al. Synthesis of Ge-Imogolite: Influence of the Hydrolysis Ratio on the Structure of the Nanotubes. *Phys. Chem. Chem. Phys.* **2011**, *13*, 14516−14522.

(8) Tenne, R. Inorganic Nanotubes and Fullerene-like Nanoparticles. *Nat. Nanotechnol.* **2006**, *1*, 103−111.

(9) Maillet, P.; Levard, C.; Spalla, O.; Masion, A.; Rose, J.; Thill, A. Growth Kinetic of Single and Double-Walled Aluminogermanate Imogolite-like Nanotubes: An Experimental and Modeling Approach. *Phys. Chem. Chem. Phys.* **2011**, *13*, 2682−2689.

(10) Mukherjee, S.; Bartlow, V. M.; Nair, S. Phenomenology of the Growth of Single-Walled Aluminosilicate and Aluminogermanate Nanotubes of Precise Dimensions. *Chem. Mater.* **2005**, *17*, 4900−4909.

(11) Yucelen, G. I.; Choudhury, R. P.; Vyalikh, A.; Scheler, U.; Beckham, H. W.; Nair, S. Formation of Single-Walled Aluminosilicate Nanotubes from Molecular Precursors and Curved Nanoscale Intermediates. *J. Am. Chem. Soc.* **2011**, *133*, 5397−5412.

(12) Farmer, B. V. C.; Fraser, R.; Tait, J. M. Synthesis of Imogolite: A Tubular Aluminium Silicate Polymer. *J. Chem. Soc., Chem. Commun.* **1977**, 462−463.

(13) Yoshinaga, N.; Aomine, S. Imogolite in Some Ando Soils. *Soil Sci. Plant Nutr.* **1962**, *8*, 22−29.

(14) Arancibia-Miranda, N. N.; Escudey, M.; Molina, M.; García-González, M. T. Use of Isoelectric Point and pH to Evaluate the

Synthesis of a Nanotubular Aluminosilicate. *J. Non-Cryst. Solids* **2011**, *357*, 1750−1756.
(15) Arancibia-Miranda, N.; Escudey, M.; Molina, M.; García-González, M. T. Kinetic and Surface Study of Single-Walled Aluminosilicate Nanotubes and Their Precursors. *Nanomaterials* **2013**, *3*, 126−140.
(16) Arancibia-Miranda, N.; Silva-Yumi, J.; Escudey, M. Effect of Cations in the Background Electrolyte on the Adsorption Kinetics of Copper and Cadmium and the Isoelectric Point of Imogolite. *J. Hazard. Mater.* **2015**, *299*, 675−684.
(17) Wada, S. Imogolite Synthesis at 25 °C. *Clays Clay Miner.* **1987**, *35*, 379−384.
(18) Avellan, A.; Levard, C.; Chaneac, C.; Borschneck, D.; Onofri, F. R. A.; Rose, J.; Masion, A.; Farmer, V. C.; Fraser, A. R.; Tait, J. M.; et al. Accelerated Microwave Assisted Synthesis of Alumino-Germanate Imogolite Nanotubes. *RSC Adv.* **2016**, *6*, 108146−108150.
(19) Denaix, L.; Lamy, I.; Bottero, J. Y. Synthetic Colloidal Amorphous Aluminosilicates and Their Precursors. *Colloids Surf., A* **1999**, *158*, 315−325.
(20) Barrett, S. M.; Budd, P. M.; Price, C. The Synthesis and Characterization of Imogolite. *Eur. Polym. J.* **1991**, *27*, 609−612.
(21) Lam, C. H.; Yang, A.-C.; Chi, H.-Y.; Chan, K.-Y.; Hsieh, C.-C.; Kang, D.-Y. Microwave-Assisted Synthesis of Highly Monodispersed Single-Walled Alunminosilicate Nanotubes. *ChemistrySelect* **2016**, *1*, 6212−6216.
(22) Boyer, M.; Paineau, E.; Bacia-Verloop, M.; Thill, A. Aqueous Dispersion State of Amphiphilic Hybrid Aluminosilicate Nanotubes. *Appl. Clay Sci.* **2014**, *96*, 45−49.
(23) Avellan, A.; Levard, C.; Kumar, N.; Rose, J.; Olivi, L.; Thill, A.; Chaurand, P.; Borschneck, D.; Masion, A. Structural Incorporation of Iron into Ge−imogolite Nanotubes: A Promising Step for Innovative Nanomaterials. *RSC Adv.* **2014**, *4*, 49827−49830.
(24) Arancibia-Miranda, N.; Escudey, M.; Pizarro, C.; Denardin, J. C.; García-González, M. T.; Fabris, J. D.; Charlet, L. Preparation and Characterization of a Single-Walled Aluminosilicate Nanotube-Iron Oxide Composite: Its Applications to Removal of Aqueous Arsenate. *Mater. Res. Bull.* **2014**, *51*, 145−152.
(25) Cradwick, P. D. G.; Farmer, V. C.; Russell, J. D.; Masson, C. R.; Wada, K.; Yoshinaga, N. Imogolite, a Hydrated Aluminium Silicate of Tubular Structure. *Nature, Phys. Sci.* **1972**, *240*, 187.
(26) Hu, J.; Kannangara, G. S. K.; Wilson, M. A.; Reddy, N. The Fused Silicate Route to Protoimogolite and Imogolite. *J. Non-Cryst. Solids* **2004**, *347*, 224−230.
(27) Wilson, M. A.; Lee, G. S. H.; Taylor, C. Tetrahedral Rehydration during Imogolite Formation. *J. Non-Cryst. Solids* **2001**, *296*, 172−181.
(28) Bottero, I.; Bonelli, B.; Ashbrook, S. E.; Wright, P. A.; Zhou, W.; Tagliabue, M.; Armandi, M.; Garrone, E. Synthesis and Characterization of Hybrid Organic/inorganic Nanotubes of the Imogolite Type and Their Behaviour towards Methane Adsorption. *Phys. Chem. Chem. Phys.* **2011**, *13*, 744−750.
(29) Maillet, P.; Levard, C.; Larquet, E.; Mariet, C.; Spalla, O.; Menguy, N.; Masion, A.; Doelsch, E.; Rose, J.; Thill, A. Evidence of Double-Walled Al-Ge Imogolite-like Nanotubes. A Cryo-TEM and SAXS Investigation. *J. Am. Chem. Soc.* **2010**, *132*, 1208−1209.
(30) Inoue, K.; Huang, P. M. Influence of Citric Acid on the Natural Formation of Imogolite. *Nature* **1984**, *308*, 58−60.
(31) Levard, C.; Masion, A.; Rose, J.; Doelsch, E.; Borschneck, D.; Dominici, C.; Ziarelli, F.; Bottero, J. Y. Synthesis of Imogolite Fibers from Decimolar Concentration at Low Temperature and Ambient Pressure: A Promising Route for Inexpensive Nanotubes. *J. Am. Chem. Soc.* **2009**, *131*, 17080−17081.
(32) Abidin, Z.; Matsue, N.; Henmi, T. Differential Formation of Allophane and Imogolite: Experimental and Molecular Orbital Study. *J. Comput.-Aided Mater. Des.* **2007**, *14*, 5−18.
(33) Yucelen, G. I.; Kang, D. Y.; Guerrero-Ferreira, R. C.; Wright, E. R.; Beckham, H. W.; Nair, S. Shaping Single-Walled Metal Oxide Nanotubes from Precursors of Controlled Curvature. *Nano Lett.* **2012**, *12*, 827−832.
(34) McCutcheon, A.; Hu, J.; Kamali Kannangara, G.; Wilson, M.; Reddy, N. ^{29}Si Labelled Nanoaluminosilicate Imogolite. *J. Non-Cryst. Solids* **2005**, *351*, 1967−1972.
(35) Bonelli, B.; Bottero, I.; Ballarini, N.; Passeri, S.; Cavani, F.; Garrone, E. IR Spectroscopic and Catalytic Characterization of the Acidity of Imogolite-Based Systems. *J. Catal.* **2009**, *264*, 15−30.
(36) Gil, B.; Zones, S. I.; Hwang, S.; Bejblova, M. Acidic Properties of SSZ-33 and SSZ-35 Novel Zeolites: A Complex Infrared and MAS NMR Study. *J. Phys. Chem. C* **2008**, *112*, 2997−3007.
(37) Li, Y.; Cheng, X.; Cao, W.; Gong, L.; Zhang, R.; Zhang, H. Fabrication of Adiabatic Foam by Sodium Silicate with Glass Fiber as Supporting Body. *Constr. Build. Mater.* **2016**, *112*, 933−939.
(38) Chen, Y.; Hong, Y.; Zheng, F.; Li, J.; Wu, Y.; Li, L. Preparation of silicate stalagmite from sodium silicate. *J. Alloys Compd.* **2009**, *478*, 411−414.
(39) Amara, M.-S.; Paineau, E.; Bacia-Verloop, M.; Krapf, M.-E. M.; Davidson, P.; Belloni, L.; Levard, C.; Rose, J.; Launois, P.; Thill, A. Single-Step Formation of Micron Long $(OH)_3Al_2O_3Ge(OH)$ Imogolite-like Nanotubes. *Chem. Commun.* **2013**, *49*, 11284−11286.
(40) Lee, H.; Jeon, Y.; Lee, Y.; Lee, S. U.; Takahara, A.; Sohn, D. Thermodynamic Control of Diameter-Modulated Aluminosilicate Nanotubes. *J. Phys. Chem. C* **2014**, *118*, 8148−8152.
(41) Marzan, L. L.; Philipse, A. P. Synthesis of Platinum Nanoparticles in Aqueous Host Dispersions of Inorganic (Imogolite) Rods. *Colloids Surf., A* **1994**, *90*, 95−109.
(42) Yucelen, G. I.; Kang, D.-Y.; Schmidt-Krey, I.; Beckham, H. W.; Nair, S. A Generalized Kinetic Model for the Formation and Growth of Single-Walled Metal Oxide Nanotubes. *Chem. Eng. Sci.* **2013**, *90*, 200−212.
(43) Yucelen, G. I.; Choudhury, R. P.; Leisen, J.; Nair, S.; Beckham, H. W. Defect Structures in Aluminosilicate Single-Walled Nanotubes: A Solid-State Nuclear Magnetic Resonance Investigation. *J. Phys. Chem. C* **2012**, *116*, 17149−17157.
(44) Jolivet, J.-P.; Chanéac, C.; Chiche, D.; Cassaignon, S.; Durupthy, O.; Hernandez, J. Basic Concepts of the Crystallization from Aqueous Solutions: The Example of Aluminum Oxy(hydroxi)des and Aluminosilicates. *C. R. Geosci.* **2011**, *343*, 113−122.
(45) Levard, C.; Masion, A.; Rose, J.; Doelsch, E.; Borschneck, D.; Olivi, L.; Chaurand, P.; Dominici, C.; Ziarelli, F.; Thill, A.; Maillet, P.; Bottero, J. Y. Synthesis of Ge-Imogolite: Influence of the Hydrolysis Ratio on the Structure of the Nanotubes. *Phys. Chem. Chem. Phys.* **2011**, *13*, 14516−14522.
(46) Davis, J. A.; James, R. O.; Leckie, J. O. Surface Ionization and Complexation at the Oxide/water Interface: I. Computation of Electrical Double Layer Properties in Simple Electrolytes. *J. Colloid Interface Sci.* **1978**, *63*, 480−499.
(47) Davis, J. A.; Leckie, J. O. Surface Ionization and Complexation at the Oxide/water Interface. 3. Adsorption of Anions. *J. Colloid Interface Sci.* **1980**, *74*, 32−43.
(48) Davis, J. A.; Leckie, J. O. Surface Ionization and Complexation at the Oxide/water Interface II. Surface Properties of Amorphous Iron Oxyhydroxide and Adsorption of Metal Ions. *J. Colloid Interface Sci.* **1978**, *67*, 90−107.
(49) Jara, A. A.; Goldberg, S.; Mora, M. L. Studies of the Surface Charge of Amorphous Aluminosilicates Using Surface Complexation Models. *J. Colloid Interface Sci.* **2005**, *292*, 160−170.
(50) Kosmulski, M. pH-Dependent Surface Charging and Points of Zero Charge. III. Update. *J. Colloid Interface Sci.* **2006**, *298*, 730−741.
(51) Lee, S. U.; Choi, Y. C.; Youm, S. G.; Sohn, D. Origin of the Strain Energy Minimum in Imogolite Nanotubes. *J. Phys. Chem. C* **2011**, *115*, 5226−5231.
(52) Zhao, M.; Xia, Y.; Mei, L. Energetic Minimum Structures of Imogolite Nanotubes: A First-Principles Prediction. *J. Phys. Chem. C* **2009**, *113*, 14834−14837.
(53) Demichelis, R.; Noël, Y.; D'Arco, P.; Maschio, L.; Orlando, R.; Dovesi, R. Structure and Energetics of Imogolite: A Quantum Mechanical Ab Initio Study with B3LYP Hybrid Functional. *J. Mater. Chem.* **2010**, *20*, 10417.

DOI: 10.1021/acs.jpcc.6b12155
J. Phys. Chem. C 2017, 121, 12658−12668

(54) Guimarães, L.; Enyashin, A. N.; Frenzel, J.; Heine, T.; Duarte, H. A.; Seifert, G. Imogolite Nanotubes: Stability, Electronic, and Mechanical Properties. *ACS Nano* **2007**, *1*, 362−368.
(55) González, R. I.; Ramírez, R.; Rogan, J.; Valdivia, J. A.; Munoz, F.; Valencia, F.; Ramírez, M.; Kiwi, M. Self-Rolling of an Aluminosilicate Sheet into a Single Walled Imogolite Nanotube: The Role of the Hydroxyl Arrangement. *AIP Conf. Proc.* **2015**, *1702*, 050004.
(56) Lourenço, M. P.; Guimarães, L.; Da Silva, M. C.; De Oliveira, C.; Heine, T.; Duarte, H. A. Nanotubes with Well-Defined Structure: Single- and Double-Walled Imogolites. *J. Phys. Chem. C* **2014**, *118*, 5945−5953.
(57) Alvarez-Ramírez, F. Ab Initio Simulation of the Structural and Electronic Properties of Aluminosilicate and Aluminogermanate Natotubes with Imogolite-like Structure. *Phys. Rev. B: Condens. Matter Mater. Phys.* **2007**, *76*, 1−14.
(58) Li, L.; Xia, Y.; Zhao, M.; Song, C.; Li, J.; Liu, X. The Electronic Structure of a Single-Walled Aluminosilicate Nanotube. *Nanotechnology* **2008**, *19*, 175702.
(59) Gustafsson, J. P. The Surface Chemistry of Imogolite. *Clays Clay Miner.* **2001**, *49*, 73−80.
(60) Kresse, G.; Furthmüller, J. Efficient Iterative Schemes for *Ab Initio* Total-Energy Calculations Using a Plane-Wave Basis Set. *Phys. Rev. B: Condens. Matter Mater. Phys.* **1996**, *54*, 11169−11186.
(61) Kresse, G.; Furthmüller, J. Efficiency of Ab-Initio Total Energy Calculations for Metals and Semiconductors Using a Plane-Wave Basis Set. *Comput. Mater. Sci.* **1996**, *6*, 15−50.
(62) Perdew, J. P.; Burke, K.; Ernzerhof, M. Generalized Gradient Approximation Made Simple. *Phys. Rev. Lett.* **1996**, *77*, 3865−3868.
(63) Plimpton, S. Fast Parallel Algorithms for Short-Range Molecular Dynamics. *J. Comput. Phys.* **1995**, *117*, 1−19.
(64) van Duin, A. C. T.; Dasgupta, S.; Lorant, F.; Goddard, W. A., III Reaxff: A reactive force field for hydrocarbons. *J. Phys. Chem. A* **2001**, *105*, 9396−9409.
(65) Bai, C.; Liu, L.; Sun, H. Molecular Dynamics Simulations of Methanol to Olefin Reactions in HZSM-5 Zeolite Using a ReaxFF Force Field. *J. Phys. Chem. C* **2012**, *116*, 7029−7039.
(66) Psofogiannakis, G. M.; McCleerey, J. F.; Jaramillo, E.; van Duin, A. C. T. ReaxFF Reactive Molecular Dynamics Simulation of the Hydration of Cu-SSZ-13 Zeolite and the Formation of Cu Dimers. *J. Phys. Chem. C* **2015**, *119*, 6678−6686.
(67) Liu, L.; Jaramillo-Botero, A.; Goddard, W. A.; Sun, H. Development of a ReaxFF Reactive Force Field for Ettringite and Study of Its Mechanical Failure Modes from Reactive Dynamics Simulations. *J. Phys. Chem. A* **2012**, *116*, 3918−3925.
(68) Ramírez, M.; González, R. I.; Munoz, F.; Valdivia, J. A.; Rogan, J.; Kiwi, M. *Coaxial Nanocable Composed by Imogolite and Carbon Nanotubes*; AIP Publishing: 2015; Vol. *1702*, p 50005.

DOI: 10.1021/acs.jpcc.6b12155
J. Phys. Chem. C 2017, 121, 12658−12668